doi:10.1093/plphys/kiab424 PLANT PHYSIOLOGY 2021: 187: 2110–2125

Plant Physiology®

Research Report

# Two plastid POLLUX ion channel-like proteins are required for stress-triggered stromal $Ca^{2+}$ release

Carsten Völkner,[1] Lorenz Josef Holzner ,[2] Philip M. Day,[1] Amra Dhabalia Ashok,[3,4] Jan de Vries,[3,4,5,6] Bettina Bölter[2] and Hans-Henning Kunz [1,2,*,†]

1 School of Biological Sciences, Washington State University, Pullman, WA 99164-4236, USA
2 Department of Plant Biochemistry, LMU Munich, 82152 Planegg-Martinsried, Germany
3 Department of Applied Bioinformatics, University of Goettingen, Institute for Microbiology and Genetics, 37077 Göttingen, Germany
4 International Max Planck Research School for Genome Science, 37077 Göttingen, Germany
5 Applied Bioinformatics, Goettingen Center for Molecular Biosciences (GZMB), University of Goettingen, Göttingen, Germany
6 Campus Institute Data Science (CIDAS), University of Goettingen, 37077 Göttingen, Germany

*Author for communication: kunz@lmu.de
†Senior author.

H.-H.K. designed research and wrote the manuscript. C.V. performed most experiments, assisted in writing, and analyzed data. L.J.H. performed BN electrophoresis. P.M.D. purified α-PEC1 antigen. A.D.A. and J.d.V. analyzed PEC phylogeny, B.B. carried out protein import, membrane fractionation, and PEC topology studies. All authors assisted in editing the manuscript.

The author responsible for distribution of materials integral to the findings presented in this article in accordance with the policy described in the Instructions for Authors (https://academic.oup.com/plphys/pages/General-Instructions) is Hans-Henning Kunz.

## Abstract

Two decades ago, large cation currents were discovered in the envelope membranes of *Pisum sativum* L. (pea) chloroplasts. The deduced $K^+$-permeable channel was coined fast-activating chloroplast cation channel but its molecular identity remained elusive. To reveal candidates, we mined proteomic datasets of isolated pea envelopes. Our search uncovered distant members of the nuclear POLLUX ion channel family. Since pea is not amenable to molecular genetics, we used *Arabidopsis thaliana* to characterize the two gene homologs. Using several independent approaches, we show that both candidates localize to the chloroplast envelope membrane. The proteins, designated PLASTID ENVELOPE ION CHANNELS (PEC1/2), form oligomers with regulator of $K^+$ conductance domains protruding into the intermembrane space. Heterologous expression of PEC1/2 rescues yeast mutants deficient in $K^+$ uptake. Nuclear POLLUX ion channels cofunction with $Ca^{2+}$ channels to generate $Ca^{2+}$ signals, critical for establishing mycorrhizal symbiosis and root development. Chloroplasts also exhibit $Ca^{2+}$ transients in the stroma, probably to relay abiotic and biotic cues between plastids and the nucleus via the cytosol. Our results show that *pec1pec2* loss-of-function double mutants fail to trigger the characteristic stromal $Ca^{2+}$ release observed in wild-type plants exposed to external stress stimuli. Besides this molecular abnormality, *pec1pec2* double mutants do not show obvious phenotypes. Future studies of PEC proteins will help to decipher the plant's stress-related $Ca^{2+}$ signaling network and the role of plastids. More importantly, the discovery of PECs in the envelope membrane is another critical step towards completing the chloroplast ion transport protein inventory.

Received March 09, 2021. Accepted August 11, 2021. Advance access publication September 7, 2021

## Introduction

Land plants cannot escape from environmental challenges collectively known as abiotic and biotic stress. Consequently, evolutionary innovations in the molecular mechanisms to sense and respond to rapidly changing conditions likely played a key role in the success of land plants (Furst-Jansen et al., 2020). Leaf plastids are optimized for light harvesting, rendering the organelle a sensory hub to collect information about the plant's environment. Chloroplasts employ several mechanisms to transmit environmental information to the nucleus to adjust gene expression. These include changes in metabolite and hormone levels, redox potential, reactive oxygen species production, and ion flux. Through the action of ion channels and carriers, signals—encoded as ion transients—can be relayed within seconds. The best-known ion signals are $Ca^{2+}$ transients which exist in plastids and several other organelles, including the nucleus (Resentini et al., 2021).

In the nuclear envelope, $Ca^{2+}$ and $K^+$ transport are coupled (Charpentier et al., 2016). The, $Ca^{2+}$ channel CYCLIC NUCLEOTIDE-GATED CHANNEL 15 functionally interacts with Doesn't Make Infections 1 (DMI), a member of the CASTOR/POLLUX/DMI ion channel family. Both channels work in concert to trigger $Ca^{2+}$ transients critical for root development and in some species mycorrhizal symbiosis (Charpentier et al., 2016; Leitao et al., 2019). In the plastid envelope, a similar system may exist as the organelle elicits stromal $Ca^{2+}$ transients in response to various triggers such as sodium chloride (NaCl) and osmotic shock (Nomura et al., 2012), temperature changes (Lenzoni and Knight, 2019), and circadian rhythms (Marti Ruiz et al., 2020). However, the inventory of ion transport proteins in the inner envelope (IE) membrane of plastids is still incomplete. Only recently, the dual-targeted mitochondrial calcium uniporter cMCU has been discovered, and reportedly plays a role in $Ca^{2+}$ flux into mitochondria and mature chloroplasts (Teardo et al., 2019). Indeed, *cmcu* loss-of-function mutants show dampened stromal $Ca^{2+}$ flux in response to osmotic but not salt-stress (Teardo et al., 2019). Because significant stromal $Ca^{2+}$ transients remain in *cmcu*, other ion channels and/or $Ca^{2+}$ transporters are expected in the plastid IE membrane (Resentini et al., 2021). The CHLOROPLAST MANGANESE TRANSPORTER 1/BIVALENT CATION TRANSPORTER 2 (CMT1/BICAT2) transporter was suggested as an alternative IE $Ca^{2+}$ transporter as its absence impacts the shape of stromal $Ca^{2+}$ release after dark transition (Frank et al., 2019). However, other data indicate that this particular carrier may primarily transport $Mn^{2+}$ ions (Eisenhut et al., 2018; Zhang et al., 2018).

Knowledge about plastid $K^+$ flux across the IE is similar limited. Thus far, only two $K^+/H^+$ exchangers from the K efflux antiporter (KEA) family have been characterized in more detail (Aranda-Sicilia et al., 2012; Kunz et al., 2014). Both carriers (KEA1 and KEA2) physiologically function in pH and ion homeostasis which is critical for plastid gene expression and development (Aranda Sicilia et al., 2021; deTar et al., 2021). The IE membrane potential of at least −70 mV on the stromal side (Wu et al., 1991) makes $K^+/H^+$ valves such as KEA1/2 a necessity for osmoregulation to balance $K^+$ influx and prevent rupture of plastids (Bernardi, 1999). To functionally describe IE cation channel(s) that aid in ion influx, reconstituted proteins from *Spinacia oleracea* L. (spinach) (Wang et al., 1993; Mi et al., 1994) or *Pisum sativum* L. (pea) (Pottosin et al., 2005) chloroplasts were employed in electrophysiological studies; these efforts resulted in the characterization of the voltage-dependent fast-activating chloroplast cation (FACC) channel of pea chloroplasts (Pottosin et al., 2005). The channel exhibits conductivity for $K^+ > Na^+ > Ca^{2+} \geqslant Mg^{2+}$ ions. While the experimental setup seemed to assure that the channel(s)' activity originated from the IE membrane (Pottosin and Dobrovinskaya, 2015), it is not entirely clear if the currents came exclusively from a single channel type. Fifteen years later, no FACC channel gene candidate(s) has emerged to explain what protein(s) may have caused the recorded $K^+$ currents in patch-clamped pea chloroplasts.

In this study, we set out to identify first candidate proteins and their corresponding genetic loci that may explain the recorded $K^+$ and other cation currents in the chloroplast IE membrane. By mining proteomic data on pea and *Arabidopsis thaliana* leaf plastids, distant members of the CASTOR/POLLUX/DMI ion channel family emerged as potential FACC candidates. Therefore, the goal of this study was to (1) determine if leaf plastids indeed possess members from the CASTOR/POLLUX ion channel family, (2) gain initial insights into their physiological relevance through heterologous expression in yeast and the study of *A. thaliana* loss-of-function mutants, and (3) test if plastid $Ca^{2+}$ transients depend on the activity of CASTOR/POLLUX-like ion channels.

## Results and discussion

### The family of CASTOR/POLLUX cation channels contains functionally similar members with plastid transit peptides

To identify potential FACC candidates, we mined published pea chloroplast envelope proteome datasets (Brautigam et al., 2008; Gutierrez-Carbonell et al., 2014). Only four different protein types related to ion transport were found: putative metal-transporting P-type ATPase PAA1, glutathione-regulated potassium-efflux system protein (KEA), Voltage-dependent anion-selective channel protein (VDAC), and probable ion channel CASTOR-like (Psat6g113560). PAA1 and KEA represent well-characterized copper and respectively $K^+$ carriers (Shikanai et al., 2003; Aranda-Sicilia et al., 2012; Kunz et al., 2014; Tsujii et al., 2019) and are therefore unlikely responsible for FACC-mediated currents. A frequent contaminant in plastid proteomics, VDAC is an anion-selective channel in the mitochondrial outer membrane (Clausen et al., 2004). However, a protein annotated "probable ion channel CASTOR-like" was intriguing as CASTOR/POLLUX/DMI have been described as nuclear cation channels with


**Figure 1** Phylogenetic tree of PEC/CASTOR/POLLUX family members. Phylogenetic framework for the evolutionary history of PEC, CASTOR, and POLLUX. Homologs of PEC, CASTOR, and POLLUX were sampled from genomes of 17 land plants, 7 streptophyte algae, and 4 chlorophytes. We further added *in silico* translated homologs from the transcriptomes of *Spirogyra pratensis* (de Vries et al., 2020), *Coleochaete scutata and Zygnema circumcarinatum* (de Vries et al., 2018), and *Coleochaete orbicularis* (Ju et al., 2015). Thirteen animal streptolysin O (SLO1) sequences were included as an out-group (blue). Only protein sequences longer than 700 AAs were included in the analysis. A rooted maximum likelihood phylogeny of all 170 sequences was computed using LG + F + R7 as model for protein evolution (chosen according to BIC). A 1,000 ultrafast bootstrap (UFBoot2; Hoang et al., 2018) replicates were computed. Only ultrafast bootstrap values $\geqslant$50 are shown and full support (ultrafast bootstrap values of 1,000) is depicted by a filled dot. PEC, CASTOR, and POLLUX sequences are found across the green lineage (fully supported yellow clade) and were likely present as a single-copy ortholog in the last common ancestor of Chloroplastida. Early during streptophyte evolution, the PEC/CASTOR/POLLUX ortholog duplicated, giving rise to the clade of streptophyte PECs (hues of orange) and CASTOR/POLLUX (hues of teal green). Scale bar length corresponds to 2.0 expected substitutions per site.

conductance for $K^+$, $Rb^+$, $Na^+$, and $Ca^{2+}$ (Charpentier et al., 2008; Venkateshwaran et al., 2012; Kim et al., 2019). We designated the candidate PEC. To understand the evolutionary history of PEC, POLLUX, and CASTOR, we performed a phylogenetic analysis (Figure 1). We used: (1) POLLUX, CASTOR, and DMI proteins from *L. japonicus*, *M. truncatula*, *Pisum sativum*, and *O.a sativa*; (2) PEC proteins from *A. thaliana* (At5g02940, At5g43745) as query in a BLASTp search against a dataset of 17 land plants, 11 streptophyte algae, and 4 chlorophyte algae. Among these 31 chloroplastida, we detected 157 homologs with a minimum length of 700 amino acids (AAs). These long homologs were used in all following analyses; the topology stayed robust when we included shorter sequences (Supplemental Figure S1). PEC's structural similarity to the SLO big potassium channel family (Roy et al., 2010), led us to add 13 animal SLO sequences as an outgroup.

All homologs of PEC, POLLUX, and CASTOR fell into a fully supported clade of diverse sequences from chloroplastida (Figure 1). In this large Chloroplastida clade, a few chlorophyte homologs branch sister to all other streptophyte sequences. The sequences from streptophytes (forming a subclade, bootstrap support of 87) were distributed over two major clades: a PEC clade and a CASTOR/POLLUX clade. Homologs of PEC fell into a fully supported clade that included sequences spanning the diversity of streptophytes; we detected PEC homologs in all major classes of streptophyte algae—from those most divergent from land plants, represented by *C. atmophyticus* and *M. viride* (Wang et al., 2020)—and diverse land plants. Nested within this clade of putative streptophyte PEC proteins was an angiosperm-specific subclade, in which a PEC homolog from *A. trichopoda* (see Amborella Genome, 2013) branched sister to homologs from all other angiosperms—which is in line with its position in the species phylogeny. A duplication that gave rise to *At*PEC1 and *At*PEC2 appears specific to the genus Arabidopsis.

The large CASTOR/POLLUX clade (ultrafast bootstrap support of 91) also contained homologs from across the diversity of streptophytes; the topology of this clade largely followed the species phylogeny. Clear orthogroups of solely CASTOR and solely POLLUX first appeared in angiosperms; in each of these two clades, *Amborella* sequences branch sister to the other angiosperm sequences, suggesting a duplication event that occurred in a common ancestor of all extant angiosperms. It is noteworthy that, branching sister to the streptophyte CASTOR/POLLUX clade, we recovered a fully supported clade that contained homologs from diverse nonvascular streptophytes (including representatives of all streptophyte algae); this suggests that there was another very early duplication of the CASTOR/POLLUX ortholog followed by a loss early during vascular evolution—or euphyllophyte evolution (see Supplemental Figure S1, where a *Selaginella* homolog falls into this clade).

In sum, it appears that there was a single PEC/CASTOR/POLLUX ortholog in the last common ancestor of chloroplastida when the green lineage was in its infancy. At the base of streptophyta, this ortholog duplicated, giving rise to the clade of PECs and the clade of CASTOR/POLLUX proteins. During the course of evolution, there were some lineage-specific duplications in each of the orthogroups—including the duplication in a common ancestor of angiosperms that gave rise to the separate POLLUX and CASTOR clades. From a bird's eye view, the orthogroups of PEC and CASTOR/POLLUX are each likely as old as streptophyta.

We compared functional domains of *At*PEC1/2 with the nuclear member DMI1 using InterPro (Supplemental Figure S2A). All three proteins contain a well-conserved C-terminal CASTOR/POLLUX domain (IPR010420). This stretch includes a tandem regulator of K+ conductance (RCK) domain (IPR036721), previously determined as functionally relevant for the nuclear members (Kim et al., 2019). In the N-terminal regions the three members differ. Only PEC1/2 possess a voltage-gated potassium channel superfamily domain (SSF81324) which was not identified in DMI1. Additionally, both PEC members contain a predicted pTP (Schwacke et al., 2003; Sun et al., 2009) and were identified in recent envelope proteomes from Arabidopsis (Bouchnak et al., 2019; Trentmann et al., 2020).

## Heterologous expression of PEC1 and PEC2 rescues a $K^+$ transport deficient yeast mutant

Nuclear envelope members of the CASTOR/POLLUX cation channel family exhibit conductivity for $K^+$, $Rb^+$, $Na^+$, and $Ca^{2+}$ ions (Charpentier et al., 2008; Kim et al., 2019). Initially, we injected PEC1/2-YFP (-pTPs) cRNA into Xenopus oocytes to perform electrophysiology. However, oocytes did not synthesize the candidate proteins and PEC1/2-YFP was not detectable at the plasma membrane.

Therefore, we employed yeast in which the plasma membrane $K^+$-transportome is well-established [reviewed in (Arino et al., 2019)] and that had been successfully used as a model to study POLLUX family channels (Charpentier et al., 2008). Heterologous expression of *Lj*POLLUX restored growth of MAB2d, a yeast mutant defective in $K^+$ uptake and $K^+$ efflux across the plasma membrane (Maresova and Sychrova, 2005), at low $K^+$ (Charpentier et al., 2008). PEC1/2 (-pTPs) were cloned into the constitutive expression yeast vector pYeT. As a control, we cloned DMI1, the closest Arabidopsis homolog to *Lj*POLLUX. Resulting strains were grown overnight in $K^+$ supplemented media and washed extensively. Optical density at 600 nm ($OD_{600}$) was adjusted and cells were spotted side-by-side on media plates supplemented with increasing $K^+$ amounts from 0 mM to 25 mM KCl (Figure 2A). While the wild-type (WT) strain W303 showed strong growth at all $K^+$ levels, MAB2d + pYeT-empty vector cells were severely growth limited below 25 mM KCl in the growth medium. DMI1, the Arabidopsis homolog of *Lj*POLLUX, did not robustly restore MAB2d mutant growth at low (<25 mM) KCl levels. In contrast, PEC1 and PEC2 transformed cells were able to grow on media even without additional KCl. PEC1/2 outperformed DMI1 in the MAB2d background, suggesting that PEC1 and PEC2 may possess higher $K^+$ permeability than DMI1 in this setup.

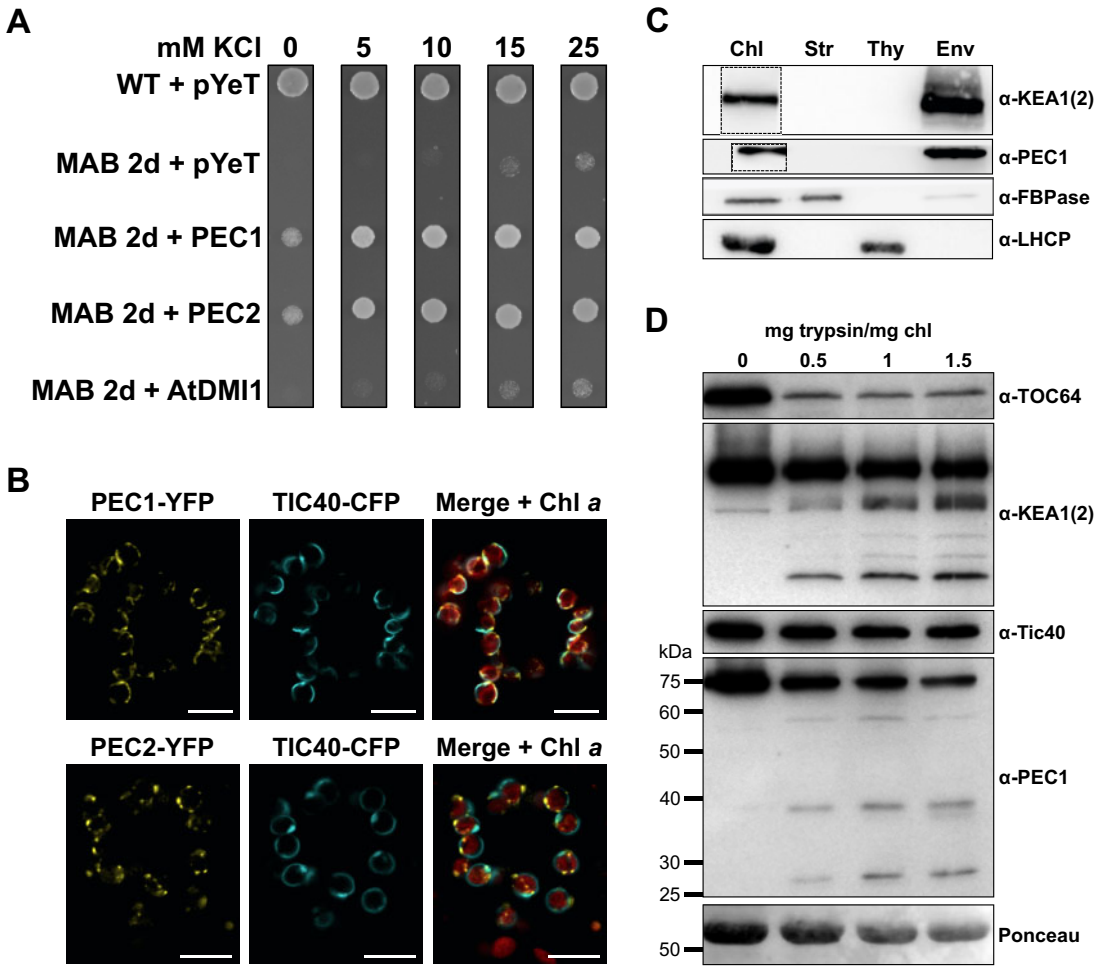


**Figure 2** PEC1 and PEC2 functional protein characterization. A, Complementation of $K^+$-uptake deficient *Saccharomyces cerevisiae* strain MAB2d with Arabidopsis POLLUX members. WT W303 cells transformed with empty pYeT vector show growth regardless of KCl concentration whereas MAB2d cells with empty pYeT vector cannot grow. PEC1 and PEC2 complement the $K^+$ uptake deficient MAB2d strain, indicating $K^+$ permeability for PEC1 and PEC2 proteins. Shown is OD 0.01 after 48 h at 30°C. B, Localization of PEC cDNA-YFP fusions to the chloroplast envelope membrane in *N. benthamiana*. Positive controls TIC40-CFP and Chl *a* confirm colocalization of PEC1 and PEC2 with the IE (scale bars = 10 μm). C, Immunoblotting of isolated chloroplast membrane fractions. Boxes indicate separate exposure time to account for relative protein abundance (Original figure Supplemental Figure S4C). Chl = entire chloroplast, Str = Stroma, Thy = Thylakoid membrane, Env = Envelope membranes (D) Protease treatment of intact WT chloroplasts. Samples were treated with 0–1.5 mg trypsin*$mg^{-1}$ chl. Samples corresponding to 10 μg chl were separated on SDS gels, blotted onto PVDF and individually immunolabeled with α-PEC1, α-KEA1(2), α-TIC40, and α-TOC64. Molecular size markers are displayed on the left of the α-PEC1 blot.

## Independent studies confirm PEC1 and PEC2 as proteins of the plastid envelope membrane

For subcellular localization studies, *PEC1/2* full-length cDNA YFP fusions were co-injected with plastid envelope marker TIC40-CFP into *Nicotiana benthamiana* leaves. The PEC1/2-YFP fluorescence signals appeared ring-shaped and overlaid with the IE marker TIC40-CFP (Figure 2B). Both signals surrounded the chlorophyll (Chl *a*) fluorescence from the thylakoids. Line plots for each fluorescence channel confirmed the spatial signal overlay (Supplemental Figure S3A). Truncated PEC1/2 variants lacking pTPs did not exhibit YFP signal around chl fluorescence but at the cell periphery (Supplemental Figure S3B). We also attempted to establish stable full-length PEC1/2-YFP overexpressor mutants in *A. thaliana*. In successfully isolated T1 individuals, YFP signal co-localized with the chl fluorescence (Supplemental Figure S3C). Unfortunately, both constructs underwent transgene silencing in the T2 generation.

Next, we radiolabeled PEC1/2 and DMI1 proteins with $^{35}$S-Met. Isolated intact chloroplasts were incubated with labeled proteins and half of each reaction thermolysin treated to degrade nonimported substrate. After electrophoresis, protein bands were visualized using a phosphorimager (Supplemental Figure S3D). For the two candidate plastid proteins PEC1/2, an additional smaller sized band was detectable in the plus and minus thermolysin lanes (see asterisks), which was absent in DMI1 lanes. The results confirm that only PEC1/2 carry pTPs which are processed by the translocon on the outer/inner chloroplast membrane (TOC–TIC) complex after import into the organelle. In

summary, independent assays led us to conclude that PEC1/2 reside in leaf plastids. It is noteworthy that the DMI homolog was initially also suggested as a plastid channel (Imaizumi-Anraku et al., 2005). However, later it was shown that this was caused by a promoter artifact and that the nuclear membrane is the genuine CASTOR/POLLUX/DMI localization (Charpentier et al., 2008).

## The C-terminal RCK domains of PEC1 reside in the envelope intermembrane space

To realize PEC1/2 immunolabeling studies we used the well-conserved C-terminal soluble stretch (≈ 64 kDa) harboring the RCK domain of PEC1 to raise serum (Supplemental Figures S2, B and S4, A). The resulting α-PEC1 almost exclusively recognized PEC1, but not PEC2 or DMI1 (Supplemental Figure S4B). Initially, we produced suborganellar fractions from *A. thaliana* chloroplasts. Immunoblotting of established marker proteins confirmed fraction purity (Figure 2C; Supplemental Figure S4C). A strong enrichment of PEC1 was identified only in the plastid envelope fraction. To probe the topology of PEC1 and the localization of the functionally critical RCK domain, intact chloroplasts were isolated from WT plants. Subsequently, isolated plastids were incubated with increasing amounts of trypsin (Figure 2D; Supplemental Figure S4D). Trypsin accesses the intermembrane space (IMS) but does not cross the IE as long as the plastids remain intact (Froehlich, 2011). TOC64, which expands from the outer envelope membrane into the cytosol, served as a control to monitor proper function of the peptidase at the cytosolic surface of the outer envelope, while KEA1/2 was used to show that trypsin entered the IMS. TIC40 is a plastid intactness indicator. The bulk of the TIC40 protein resides in the stroma and therefore only remains stable in the presence of trypsin if the IE membrane remains intact. In untreated chloroplasts, native PEC1 protein was detected at 75 kDa. In the presence of trypsin, TOC64, KEA1/2, and PEC1 were rapidly degraded while TIC40 signal remained unchanged. Because no stable PEC1 degradation product of ≈ 64 kDa accumulated, our results suggest that the long soluble PEC1 C-terminus harboring the RCK domain resides in the envelope IMS. In line with this, the heterologously expressed soluble PEC1 C-terminus was also trypsin-sensitive (Supplemental Figure S4E). It follows that PEC1 monomers likely possess an uneven number of transmembrane domains.

## In planta characterization of PEC1/2 genes and loss-of-function mutants

Initially, we inserted 2 kB PEC1/2 promoter fragments directly upstream of a GUS reporter gene. Several independent Arabidopsis lines were tested for consistent staining patterns to gain insights into what plastid types harbor PEC1 and PEC2, respectively (Figure 3A). No unspecific blue GUS staining was observed when the WT plants were incubated with X-Glu, while the pUBQ10::GUS positive control line displayed dark blue GUS stain throughout all tissues. PEC1 and PEC2 were robustly expressed at plant ages 10, 28, and 35 d (Figure 3A; Supplemental Figure S5C). While PEC1 seemed exclusively expressed in aerial tissue, pPEC2::GUS reporter lines also showed staining in seedling roots. Both loci were expressed in mature leaf and flower tissue which is in line with the robust immunoblot signal we observed when probing isolated chloroplasts with α-PEC1 (Figure 2, C and D). The GUS tissue expression patterns were generally in line with publicly available transcriptomic data (Supplemental Figure S5A and B; Kilian et al., 2007; Zhang et al., 2020) although these suggest higher *PEC1* expression in mature leaves compared to *PEC2*.

Subsequently, we isolated T-DNA insertion mutants in PEC1 and PEC2 loci (Figure 3B; Supplemental Figure S6, A and B). None of the independent *pec1 and pec2* single mutants displayed obvious phenotypes (Supplemental Figure S6C). Therefore, two independent *pec1pec2* double mutant lines were isolated by crossing respective single mutants. In both double mutants, the absence of detectable gene-specific transcripts and PEC protein was confirmed by means of RT-PCR and immunoblotting, respectively (Figure 3C and D). CASTOR/POLLUX/DMI form tetramers in *in vivo* (Kim et al., 2019). Thus, we probed the oligomeric state of PEC1 using isolated WT and *pec1pec2* mutant chloroplasts separated on blue native (BN)-PAGE (Figure 3E). Indeed, PEC1 protein gave several higher molecular bands above the 440 kDa marker, suggesting that also the distantly related POLLUX member PEC1 exists as a multimer in vivo and potentially in complex(es) with other binding partners. To characterize the *pec* single and double loss-of-function lines, mutant plants and WT controls were grown under long-day conditions (16-h/8-h day–night cycle, 150 µmol photons $m^{-2}$ $s^{-1}$). While some mutant individuals appeared slightly smaller, no statistical differences from WT were found for fresh weight and chlorophyll content (Figure 3, F–H). Additionally, several basic photosynthesis parameters ($F_v/F_M$, NPQ, and ΦPSII) were recorded by pulse-amplitude-modulation (PAM) fluorometry (Figure 3, I and J). Again, we detected no differences from WT in any of the photosystem-II-related parameters. This indicates that the lack of PEC1 and PEC2 neither impacts photosynthesis nor chloroplast function under normal growth conditions—a striking difference from envelope $K^+/H^+$ exchanger mutants *kea1kea2* (Kunz et al., 2014; deTar et al., 2021) but also from $Mn^{2+}/Ca^{2+}$ carrier deficient *cmt1/bicat2* lines (Eisenhut et al., 2018; Zhang et al., 2018; Frank et al., 2019). Because of the importance of plastid ion carriers and their impact on the leaf ionome, several mutants show aberrations from the WT in ionomics experiments (Shikanai et al., 2003; Eisenhut et al., 2018; Zhang et al., 2018; Höhner et al., 2019). Therefore, we analyzed leaf element levels but did not find significant changes between WT and the two *pec1pec2* loss-of-function lines (Table 1). We reckoned that the lack of phenotypic abnormalities and quantitative changes of leaf elements along with intact photosynthesis may point towards a more specialized role for PEC1/2 channels such as in signaling pathways triggered by specific stress conditions.

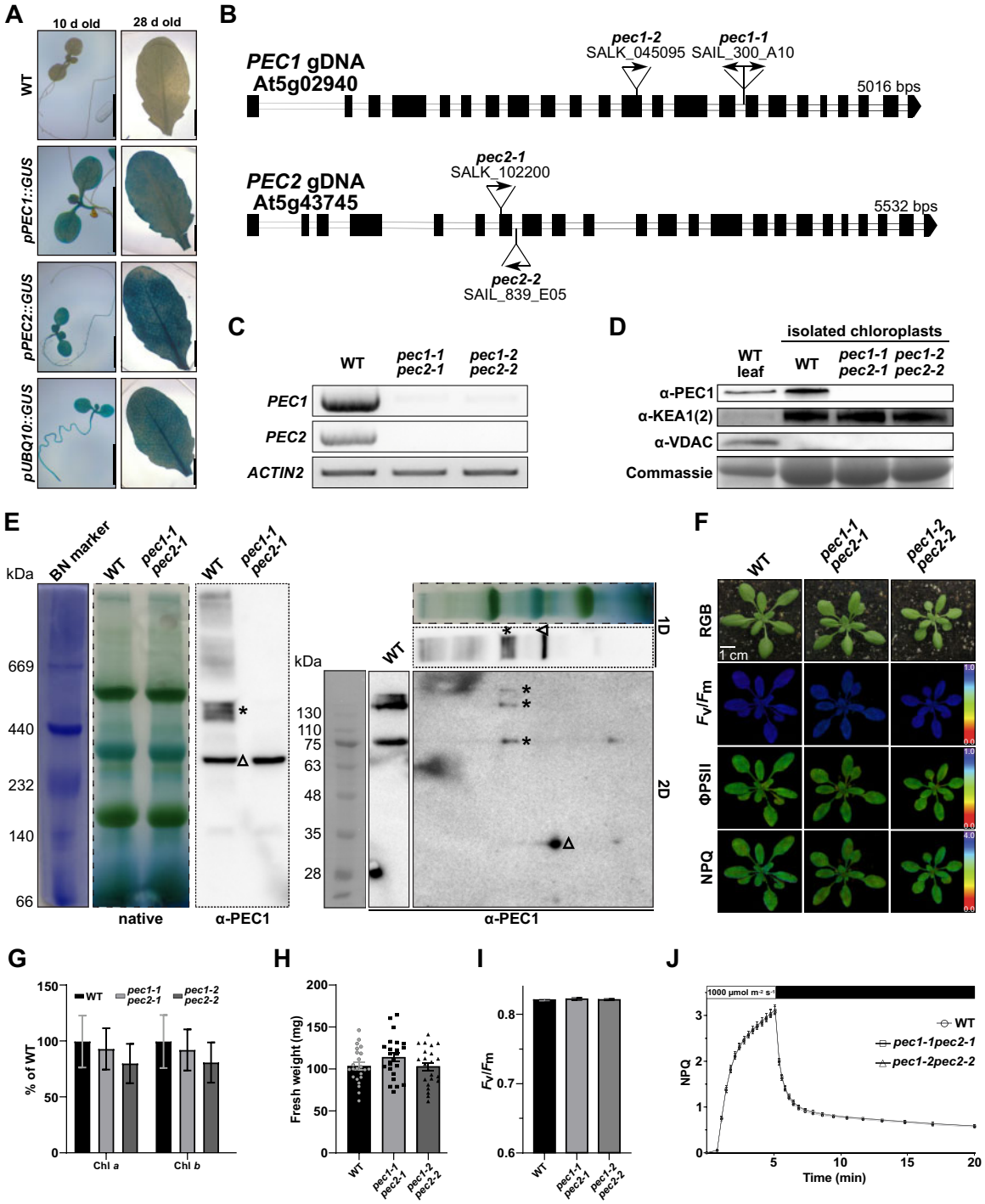


**Figure 3** PEC expression and loss-of-function mutant characterization. A, Promotor studies of *pPEC1/2::GUS* constructs indicate strong expression in *A. thaliana* tissues. Left part shows 10-d-old seedlings, right part leaves of 28-d-old plants. Experiments were repeated three times with similar results. Representative images are shown (scale bars = 5 mm). B, PEC1 and PEC2 locus information, including T-DNA insertion sites for all *pec* mutants isolated in this study. Border sequences of T-DNA insertion sites are provided in (Supplemental Figure S6C) Full-length semi-quantitative reverse transcriptase PCR shows absence of PEC1 and PEC2 transcripts in the two independent *pec1pec2* lines. D, Immunoblotting of WT and *pec1pec2* mutant proteins validates lack of PEC1(2) in the mutant plastids. α-KEA1(2) and commassie are presented as loading controls, α-VDAC confirms absence of mitochondrial contamination in the isolated chloroplast fraction. E, BN-PAGE of WT and *pec1-1pec2-1* isolated chloroplasts. Specific signals in WT samples detected by α-PEC1 are marked with asterisks. An unspecific band appearing in WT and knockout lanes was marked with triangle (Δ), which was confirmed by 2D SDS–PAGE of the WT BN lane (striped border). F, RBG and false color panel of photosynthesis measurements of WT and two *pec1pec2* double mutants. No obvious phenotypes could be detected when grown under long-day conditions at 150 µmol $m^{-2}$ $s^{-1}$ (scale bar = 1 cm). G, Normalized chlorophyll values are unchanged when compared to the WT as determined by analysis of variance and Dunn's multiple comparisons test ($P > 0.05$, mean ± SEM, $n = 9$). H, Loss of PEC1/2 does not affect plant fresh weight. Shown are pooled results of three independent experiments (mean ± SEM, $n = 23$). Photosynthetic parameters [$F_v/F_m$ (I) and NPQ kinetics (J)] are unchanged in *pec1pec2* mutants (mean ± SD, $n = 8$, a representative result of three experiments is shown).

**Table 1** Leaf-level concentrations of elements (mg*g $DW^{-1}$). Mean leaf concentration of assorted elements normalized to dry weight (mg*g $DW^{-1}$) (± SEM, $n$ = 6-7). No significance was determined using ANOVA and Tukey's multiple comparisons test ($p > 0.05$)

| Element | WT | | *pec1-1pec2-1* | | *pec1-2pec2-2* | |
|---|---|---|---|---|---|---|
| | Mean | SEM | Mean | SEM | Mean | SEM |
| P | 10.233 | 0.305 | 10.432 | 0.247 | 10.369 | 0.205 |
| S | 10.184 | 0.279 | 9.902 | 0.220 | 10.444 | 0.254 |
| Cl | 0.101 | 0.007 | 0.104 | 0.01 | 0.144 | 0.013 |
| K | 38.482 | 0.502 | 40.222 | 0.707 | 40.544 | 1.352 |
| Ca | 49.014 | 1.231 | 51.130 | 0.87 | 51.160 | 2.282 |
| Mn | 0.028 | 0.004 | 0.03 | 0.005 | 0.03 | 0.005 |
| Fe | 0.083 | 0.006 | 0.08 | 0.006 | 0.079 | 0.004 |
| Cu | 0.004 | 0.000 | 0.005 | 0.001 | 0.008 | 0.003 |
| Zn | 0.097 | 0.003 | 0.095 | 0.003 | 0.108 | 0.004 |
| Rb | 0.021 | 0.005 | 0.023 | 0.006 | 0.025 | 0.006 |
| Sr | 0.143 | 0.014 | 0.15 | 0.016 | 0.147 | 0.016 |

Mean leaf concentration of assorted elements normalized to dry weight (mg*g $DW^{-1}$) (±SEM, $n$ = 6-7). No significance was determined using analysis of variance and Tukey's multiple comparisons test ($p > 0.05$)

## The loss of PEC1/PEC2 function affects stress-induced stromal $Ca^{2+}$ transients

Chloroplasts harbor the $Ca^{2+}$ sensor protein CaS and are therefore an integral part of cellular $Ca^{2+}$ signaling (Weinl et al., 2008). Because of the involvement of CASTOR/POLLUX channels in the formation of nuclear $Ca^{2+}$ transients, it was important to test if PEC proteins may function in plastid $Ca^{2+}$ signaling.

A homozygous WT reporter line expressing stromal targeted YFP-AEQUORIN [NADPH-dependent thioredoxin reductase C (NTRC) pTP fused to YFP-AEQUORIN, therefore NTRC-YA (Mehlmer et al., 2012)] was introgressed into *pec1 and pec2* single mutants and into both *pec1pec2* double mutant lines. The same sensor line was also crossed into the *cas-1* (Nomura et al., 2012) mutant to aid as an assay control. Proper stromal localization and homogenous expression of the stromal $Ca^{2+}$ reporter was verified for all lines by microscopy (Figure 4A; Supplemental Figure S7C). Additionally, we verified similar YFP-AEQUORIN levels via RT-PCR and immunoblotting in isolated *pec1pec2* double mutants (Figure 4, B and C).

A plate reader-based seedling assay was used to quantify free stromal $Ca^{2+}$ levels through the bioluminescence signal emitted by AEQUORIN. After overnight dark incubation with the substrate coelenterazine, each well was measured to check for background luminescence which was negligible throughout (Supplemental Figure S7A). Under the assumption that *pec* single mutants are largely redundant, we first focused on characterizing *pec1pec2* double mutants. Initially, we applied an equal volume of room temperature (RT) buffer to the seedlings to observe changes in $Ca^{2+}$ levels merely triggered by the injection method. The result was a slight increase of free stromal $Ca^{2+}$ similar in all genotypes tested (Figure 4D).

Next, we tested the two strong $Ca^{2+}$ triggers NaCl and Mannitol, and observed large $Ca^{2+}$ transients maxing out at about 550 nM in the WT. Interestingly, both independent *pec1pec2* double mutant lines exhibited a drastically lower $Ca^{2+}$ response upon elicitor application compared to WT but also compared to *pec* single mutants (Figure 4, E and F; Supplemental Figure S7, D and E). In addition to the time course, we further evaluated response parameters, such as total free stromal $Ca^{2+}$ during our measurement in the form of $Ca^{2+}$ integration and peak $Ca^{2+}$ levels. Both double mutant lines showed nearly identical but significantly lower values compared to WT regardless of parameter or elicitor. As opposed to osmotic and salt stress, cold stress response was not as uniform in the WT. Only 4 of 12 seedlings showed a distinct peak in response to the addition of ice-cold buffer, ranging from 400 to 620 nM (Figure 4G). In contrast, *pec1pec2* double knockout lines never peaked higher than 390 nM in our tests ($n$ = 36, Supplemental Figure S7B). In line with prior work (Nomura et al., 2012), the $Ca^{2+}$ response in the *cas-1* control was also dampened, yet not as extreme as reported previously. This could be explained by the differing specimen types employed (leaf discs, Nomura et al., 2012 versus seedlings, this study). Interestingly, the decrease in stromal $Ca^{2+}$ transients in *cas-1* was less pronounced than in *pec1pec2*. When the same *pec1pec2* double mutant lines were backcrossed to WT, resulting F1 progenies exhibited a clear but not full recovery of the $Ca^{2+}$ (Supplemental Figure S7, F and G) transients, confirming that PEC proteins play a critical role in stromal $Ca^{2+}$ kinetics. Interestingly, none of the tested stress elicitors affected homozygous *pec1pec2* double mutant growth more severely than WT (Supplemental Figure S8).

Based on the obtained results, we compiled a working model which integrates PEC1/2's suggested function with previously described $K^+$ and $Ca^{2+}$ transport proteins in the plastid IE (Figure 4H). All our experiments confirmed PEC1/2 as an IE protein which is in line with several proteomics studies from pea and Arabidopsis. *PEC1/2* expression rescues $K^+$-uptake deficient yeast mutants. Consequently, we propose that PEC1/2 can facilitate $K^+$ influx into the stroma. According to the literature chloroplasts have a membrane potential of at least −70 mV across the IE (Wu et al., 1991), allowing for cation influx through an opened, cation-selective pore down the electrical gradient. KEA1/2 balance the $K^+$ influx through $K^+/H^+$ exchange to avoid osmotic stress. Akin to the nuclear CASTOR/POLLUX/DMI cation channels, PEC1/2 function is highly relevant for organellar stress-triggered $Ca^{2+}$ transients. Regardless of the elicitor, $Ca^{2+}$ transients remained at a very low level in *pec1pec2* double mutants. Comparing the here observed $Ca^{2+}$ readings with the published data on *cmcu and cmt1/bicat2* null mutants it appears that the loss of PECs has a more general and severe impact on stromal $Ca^{2+}$ transients. This indicates two nonmutually exclusive scenarios: First, PEC proteins themselves might also facilitate $Ca^{2+}$ flux. Second, PEC proteins may affect the activity of envelope $Ca^{2+}$ transport proteins (cMCU, BICAT2 and/or unknown ones).

In regards to scenario 1: Independent studies suggest $Ca^{2+}$ permeability for nuclear CASTOR-type cation channels albeit with different quantities. While two studies found

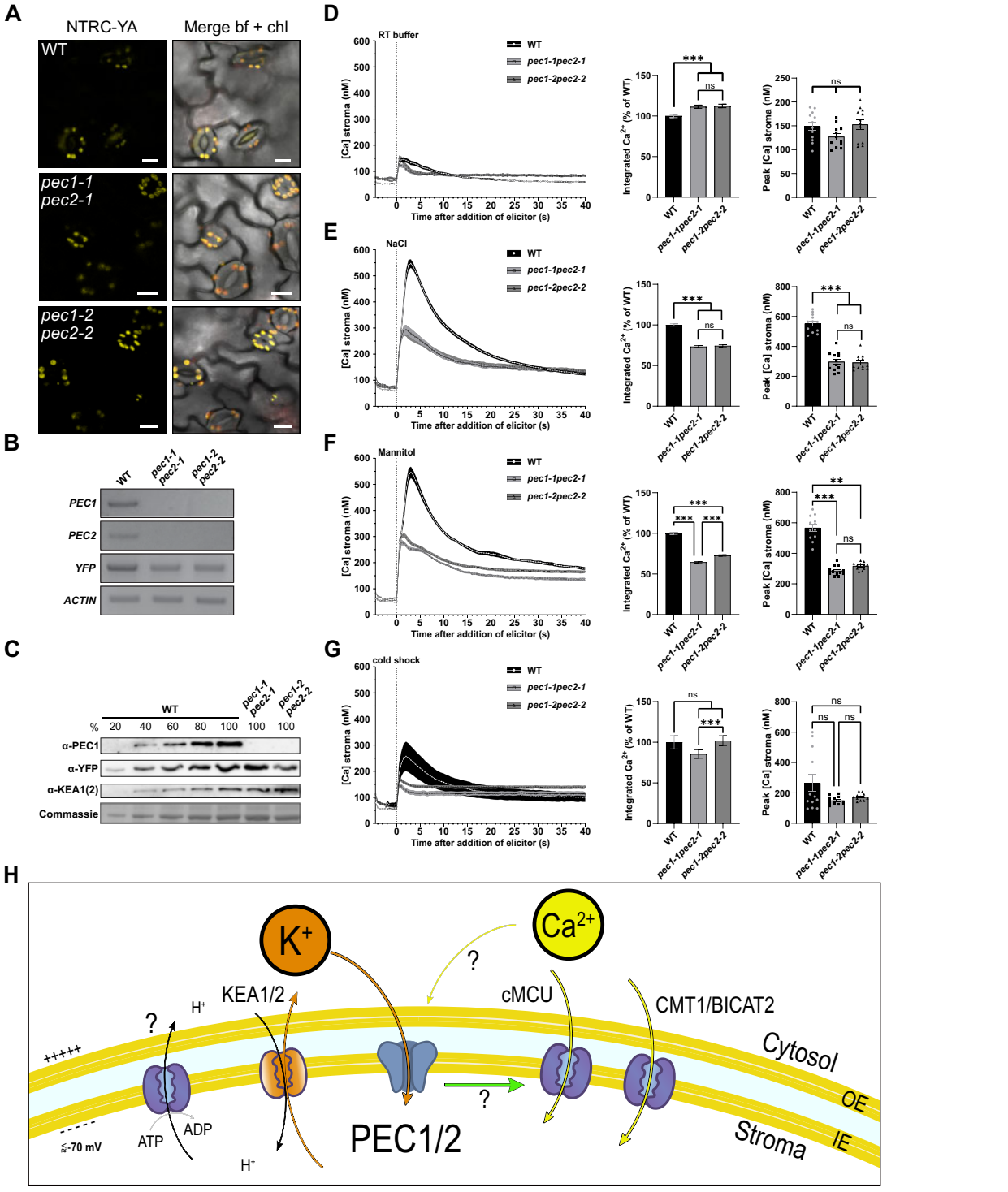


**Figure 4** Stress-triggered stromal $Ca^{2+}$ transients are diminished in *pec1pec2*. A, Plastid localization of the NTRC-YFP-AEQUORIN construct in WT and *pec1pec2* backgrounds. Representative images are shown (scale bars = 10 µm). B, Full-length semi-quantitative reverse transcriptase PCR shows absence of either PEC transcript in the two independent *pec1pec2* lines and shows similar expression of a YFP fragment that is attached to AEQUORIN. C, Immunoblotting of WT and *pec1pec2* mutant total leaf proteins shows similar YFP-AEQUORIN levels and confirms absence of PEC in *pec1pec2* mutants. Commassie and α-KEA1(2) validate similar loading for all samples. D–G, $Ca^{2+}$ transients are decreased in plants lacking plastid PEC proteins. Six-day-old seedlings were triggered with RT buffer (D) 200 mM NaCl (E) 400 mM Mannitol (F) or ice-cold buffer (G). Shown in the kinetics are the mean $Ca^{2+}$ concentrations (calculated according to Knight et al., 1996) in the stroma of 12 individuals (±SEM in the shaded area, $n = 12$). Bar graphs highlight changes in response to the respective elicitors, that is, $Ca^{2+}$ taken up into the chloroplast during the measurement (integration, relative to WT, left) and peak $Ca^{2+}$ values of the corresponding seedlings (right). Statistical differences were determined by one-way analysis of variance followed by Tukey's multiple comparisons test (mean ± SEM, $n = 12$ $^{**}P < 0.01$, $^{***}P < 0.001$). Experiments were repeated multiple times with similar results. H, Working model of $K^+$ and $Ca^{2+}$ transport mechanisms across the outer envelope and IE membrane of *A. thaliana* chloroplasts. KEA1/2 facilitate $K^+$-efflux across the IE membrane (Kunz et al., 2014). cMCU (Teardo et al., 2019) and potentially CMT1/BICAT2 (Eisenhut et al., 2018; Frank et al., 2019) aid in $Ca^{2+}$ import. PEC1/2 possess $K^+$-permeability and may impact $Ca^{2+}$ transients in the stroma through (1) having $Ca^{2+}$ conductance themselves or (2) their activity influences other envelope $Ca^{2+}$ transport proteins.

moderate preference for $K^+$ over $Rb^+$, $Na^+$, and $Ca^{2+}$ (Charpentier et al., 2008; Venkateshwaran et al., 2012), a recent structural work suggested preference for $Ca^{2+}$ over $K^+$ ions (Kim et al., 2019). Each study had to overcome technical challenges; Charpentier et al. (2008) and Venkateshwaran et al. (2012) reconstituted in vitro translated protein, whereas Kim et al. (2009) expressed CASTOR/DMI without the first two membrane domains. These limitations make it difficult to draw strong conclusions regarding the in vivo substrate of CASTOR/POLLUX/DMI cation channels. This also pertains to their plastid homologs, the PEC proteins, for which we unsuccessfully attempted electrophysiology. However, the rescue of a $K^+$ uptake deficient yeast mutant indicates that $K^+$ can pass through the PEC pore. Given the very low-level free $Ca^{2+}$ in the cytosol and stroma (low nanomolar), it seems reasonable that highly abundant $K^+$ ions (50–100 mM) represent the main PEC1/2 substrate in vivo. Notably, also the enigmatic FACC channel from pea exhibits $K^+$ and $Ca^{2+}$ conductivity (Pottosin et al., 2005).

In regards to scenario 2: PEC function may control activity of envelope $Ca^{2+}$ transport proteins. The mechanism proposed for the nuclear $Ca^{2+}$ transients controlled by CASTOR/POLLUX/DMI cation channels is unlikely to occur at the IE. In the nucleus CASTOR/POLLUX/DMI cation channels were suggested to carry counterions for the inward rectifying $Ca^{2+}$ flux. Given the literature values for the IE membrane potential of at least −70 mV the flux direction for chloroplasts should be different. Here, $K^+$ and $Ca^{2+}$ should both be drawn into the stroma by its negative voltage if facilitated by a cation channel. Therefore, the exact mechanism by which PEC activity may trigger $Ca^{2+}$ influx via the two suggested and potentially additional envelope $Ca^{2+}$ transport proteins, remains to be investigated in detail. Notably, while PEC1/2 and CMT1/BICAT2 were highly abundant in the plastid envelope proteome of Arabidopsis mesophyll chloroplasts, cMCU was not identified (Bouchnak et al., 2019; Trentmann et al., 2020). Because of cMCU's suggested cell-specific dual-targeting, the highly abundant PEC1/2 may not exert a strong impact on cMCU activity. In the future, detailed colocalization studies using endogenous promoter-driven fluorescence protein fusions and native antibodies for respective membrane proteins are needed to resolve this question.

## Conclusions

In this study, we set out to find candidate genes encoding for the enigmatic FACC channel. While we cannot say with certainty that PEC1/2 represent FACC it is likely that they contribute to the measured FACC conductance. PEC1/2 reside in the envelope membrane of pea and Arabidopsis chloroplasts and possess all characteristic functional domains of an ion channel. Similar to their homologs, the nuclear CASTOR/POLLUX/DMI cation channels, PEC1/2 restore $K^+$ flux in yeast mutants and affect the formation of organellar $Ca^{2+}$ transients. PEC1/2 might have $Ca^{2+}$ conductance themselves or their activity influences other envelope $Ca^{2+}$ transport proteins and thus impact stromal $Ca^{2+}$ transients indirectly. To resolve this, electrophysiology on reconstituted PEC proteins, colocalization, and interaction studies are needed. The discovery of PEC1/2 adds members to the chloroplast transportome and enables the understanding of $Ca^{2+}$ signaling in future work.

## Materials and Methods

### Phylogenetic analysis

We downloaded protein data from (1) genomes of seventeen land plants: *Anthoceros agrestis* as well as *Anthoceros punctatus* (Li et al., 2020), *Amborella trichopoda* (Amborella Genome, 2013), *Arabidopsis thaliana* (Lamesch et al., 2012), *Arabidopsis lyrata* (Hu et al., 2011), *Brachypodium distachyon* (International Brachypodium, 2010), *Brassica rapa* (*Brassica rapa* FPsc v1.3, DOE-JGI, http://phytozome.jgi.doe.gov/), *Gnetum montanum* (Wan et al., 2018), *Lotus japonicus* (Li et al., 2020), *Marchantia polymorpha* (Bowman et al., 2017), *Oryza sativa* (Ouyang et al., 2007), *Physcomitrium patens* (Lang et al., 2018), *Pisum sativum* (Kreplak et al., 2019), *Selaginella moellendorffii* (Banks et al., 2011), and *Sphagnum fallax* (*Sphagnum fallax* v0.5, DOE-JGI, http://phytozome.jgi.doe.gov/); protein data for *Spinacia oleracea* were obtained from (Dohm et al., 2014); (2) the genomes of seven streptophyte algae: *Chlorokybus atmophyticus* (Wang et al., 2020), *Chara braunii* (Nishiyama et al., 2018), *Klebsormidium nitens* (Hori et al., 2014), *Mesotaenium endlicherianum* (Cheng et al., 2019), *Mesostigma viride* (Wang et al., 2020), *Penium margaritaceum* (Jiao et al., 2020), *Spirogloea muscicola* (Cheng et al., 2019)—additionally, we included sequences found in the transcriptomes of *Spirogyra pratensis* (de Vries et al., 2020), *Zygnema circumcarinatum* and *Coleochaete scutata* (de Vries et al., 2018), and *Coleochaete orbicularis* (Ju et al., 2015); (3) the genomes of four chlorophytes: *Chlamydomonas reinhardtii* (Merchant et al., 2007), *Coccomyxa subellipsoidea* (Blanc et al., 2012), *Micromonas pusilla* (Worden et al., 2009), *Ulva mutabilis* (De Clerck et al., 2018).

We used (1) seed sequences from *Lotus japonicus*, *Medicago truncatula*, *Pisum sativum and Oryza sativa* and (2) animal Slo1 protein homologs from *Caenorhabditis elegans, Acanthaster planci, Danio rerio, Nematostella vectensis, Pomacea canaliculate, Echinococcus granulosus, Parasteatoda tepidariorum, Lingula anatine, Biomphalaria glabrata, Homo sapiens, Drosophila mojavensis*, and *Mus musculus* as a query sequence for a BLASTp against this dataset. Initially, we considered all homologs recovered at a cutoff level of $10^{-5}$ Alignments were generated using MAFFT v7.475 (Katoh and Standley, 2013) with an L-INS-I approach. Alignments are provided in Supplemental Datasets S1 and S2. We computed maximum likelihood phylogenies using IQ-TREE 2.0.3 (Minh et al., 2020), with 1,000 ultrafast (UFBoot2; Hoang et al., 2018) bootstrap replicates. To determine the best model, we used ModelFinder (Kalyaanamoorthy et al., 2017) and picked LG + F + R7 for Figure 1 (Le and Gascuel, 2008) and WAG + R8 (Whelan and Goldman, 2001) for Supplemental Figure S1 as the best models based on the Bayesian Information Criterion.

## Alignment and domain structure

Full-length amino acid sequences of PEC1, PEC2, and DMI1 were submitted to the InterPro protein families and domains database (https://www.ebi.ac.uk/interpro/). Figures were created using Affinity Designer (serif).

## Plant growth and isolation of Arabidopsis thaliana mutant lines

WT and mutant seeds from accession Columbia-0 (Col-0) were surface-sterilized, stratified in the dark (48 h at 4°C), and then germinated for seven days on 1/2 strength Murashige and Skoog (MS) 0.8% (w/v) phytoagar plates (pH 5.8) at 150 µmol photons $m^{-2}$ $s^{-1}$ in long-day conditions (16 h/8 h at 22°C). On day seven seedlings were transferred to soil (Sungro Professional Growing Mix #1, Sun Gro Horticulture, Agawam, MA, USA) and grown under 150 µmol photons $m^{-2}$ $s^{-1}$ illumination in 16-h/8-h day–night cycle at 22°C. Rosettes of 3-week-old plants were used for all experiments if not stated differently, except for chloroplast isolation where seeds were sown directly onto soil. All T-DNA insertion mutants were ordered from the ABRC stock center. Homozygous genotypes were confirmed by PCR using primers detailed in Supplemental Tables S1 and S2.

## Yeast complementation assay

For *Saccharomyces cerevisiae* assays, we used the MAB2d mutant (Maresova and Sychrova, 2005) and the corresponding WT strain W303. PEC1, PEC2, and DMI1 coding sequences without stop codon were cloned into the yeast expression vector pYeT, harboring a GAP promoter for strong expression and a C-terminal YFP and were transformed according via lithium acetate method (Gietz and Woods, 2001). To minimize mislocalization, the N-terminal plastid transit peptide of PEC1 and PEC2 were truncated. According to predictions of the plant proteome database (Sun et al., 2009) 44 AAs were truncated in the case of PEC1 and 50 AAs for PEC2, respectively. We observed more consistent localization of DMI1 to the plasma membrane in yeast cells, which prompted us to use the putative DMI1 signal peptide (70 AAs) as an N-terminal fusion to the PEC1/2 coding DNA sequence. Strains were grown overnight in $K^+$-supplemented dropout media, washed extensively, and shaken at 30°C for 30 min in $K^+$-free media. $OD_{600}$ was adjusted to 0.1 in water and cells were spotted side-by-side on media plates supplemented with increasing $K^+$ amounts.

## Transient *N. benthamiana* infiltration and confocal microscopy for protein localization studies

For localization studies in *N. benthamiana*, *Agrobacterium tumefaciens* strains carrying respective vectors (Supplemental Table S3) were co-injected with the 19k vector (Voinnet et al., 2003) according to (Waadt et al., 2014). Images were taken on a Leica SP8 Confocal Laser Scanning Microscope equipped with a supercontinuum laser and hybrid detectors. In co-localization experiments employing yellow fluorescent protein (YFP) and chlorophyll autofluorescence (chl *a*), both fluorophores were excited at 514 nm and recorded at 524–560 nm and 627–700 nm, respectively. Cyan fluorescent protein (CFP) was excited with a pulsed laser at 405 nm and emission was sequentially recorded at 465–492 nm.

## Promoter-GUS-activity staining

For GUS promoter fusion constructs (Supplemental Table S3), 2,000 bp 5′-fragments upstream from the respective ATG were amplified from genomic DNA and cloned into pGreenII 0179-derived vectors harboring the GUS reporter gene (Pratt et al., 2020). *Agrobacterium* containing the respective plasmids were transformed into WT plants according to (Clough and Bent, 1998). GUS staining was performed as described in (Höhner et al., 2019). Representative images are shown and experiments were carried out three times with similar results.

## Generation of α-PEC1(2) immunoglobulin

To maximize chance of recognition of the antibody against PEC1, the entire soluble domain (M244 until stop codon, ~64 kDa) was cloned into pET16b and transformed into BLR 21 for expression in *Escherichia coli*. Purification of the antigen was performed as described in (Höhner et al., 2021). An antigen solution at 0.49 mg/mL was flash-frozen on dry ice and sent for antibody generation. The PEC1 antiserum was raised in rabbits (YenZym Antibodies, San Francisco, CA, USA).

## Immunoblotting

Arabidopsis leaf tissue frozen in liquid $N_2$ was powderized using mortar and pestle. Total protein was extracted in extraction buffer [200 mM Tris pH 8.0, 4% (w/v) sodium dodecyl sulfate (SDS), 20 mM dithiothreitol (DTT)] to 0.5 g fresh weight/mL, followed by heating at 80°C for 10 min and removing insoluble debris by centrifugation at 21,000*g* for 8 min. Supernatant was mixed with Laemmli buffer and loaded on 8%–10% (w/v) acrylamide gels. A voltage of 120 V was applied until the loading dye had left the gel. Gels were either Commassie stained or electroblotted onto Polyvinylidene Fluoride (PVDF) or nitrocellulose membranes (0.45-µm pore size) by applying 70 V for 45 min. Subsequently, the membrane was incubated with blocking buffer (Tris-buffered saline with 0.05% (w/v) tween (TBS-T), 5% (w/v) nonfat dry milk) for up to 1 h at RT and incubated overnight in blocking buffer plus primary antibody at indicated dilutions, gently rocking at 4°C. Primary antibodies used in this study were α-PEC1 (this study), α-KEA1(2) (Bolter et al., 2020), α-LHCP, α-VDAC (both (Clausen et al., 2004)), α-FPBase (Benz et al., 2009), α-TIC40 (Stahl et al., 1999), α-TOC64 (Sohrt and Soll, 2000), and a commercial α-GFP antibody (Roche, Basel, Switzerland). The membrane was washed 4 times for 5 min in TBS-T and subsequently incubated with HRP conjugated secondary antibody (goat-anti-rabbit (Proteintech Cat# SA00001-2) or goat-anti-mouse in case of anti-GFP), diluted 1:10,000 in blocking buffer for 1 h at RT. The blot

was rinsed 4 times with TBS-T, 10 min each, and then developed with Biorad clarity ECL substrates (Cat#1705060) for 2–5 min. Signal was detected using a ImageQuant LAS 4000 (GE Healthcare, Chalfont St Giles, UK) with the precision setting and automatic exposure.

## Chloroplast subfractionation

Initially, chloroplasts were isolated according to (Bolter et al., 2020). Chloroplast subfractionation was performed as described in (Flores-Perez and Jarvis, 2017), with slight modifications. Intact chloroplasts were isolated, then incubated in 10 mM HEPES/KOH, 5 mM $MgCl_2$ plus complete protease inhibitor (cpi) at a concentration of 1 mg/mL chl for 30 min on ice and then ruptured by 50 strokes in a dounce homogenizer. The homogenate was loaded onto a step sucrose gradient (0.46 M, 1.0 M, 1.2 M sucrose in lysis buffer) and centrifuged at 58,000*g* for 2 h at 4°C. Stroma was collected from the top and directly used for SDS–PAGE. The envelope fraction was taken from the interface between 0.46 M and 1.0 M sucrose, diluted 1:4 with lysis buffer and centrifuged for 30 min at 256,000*g* at 4°C. The resulting pellet was resuspended in loading buffer. Thylakoids were recovered from the pellet of the gradient, washed 5 times in lysis buffer. Loading was adjusted to total protein.

## Protease treatments of chloroplasts

For trypsin treatment of intact chloroplasts an equivalent of 100 μg chl was pelleted and resuspended in 100 μL wash buffer supplemented with 0.5 mM $CaCl_2$. Trypsin was added in the indicated amounts per milligram chl and incubated for 45 min at 23°C. The treatment was terminated by addition of 1 × cpi, chloroplasts were reisolated by centrifugation and washed once with wash buffer + 1 × cpi. The final pellet was solubilized in Laemmli loading buffer containing 2 M urea and 1 × cpi, heated at 65°C for 5 min and plastids equivalent to 10 μg chl were loaded onto an SDS gel followed by immunoblotting as described above. All experiments were at least done in triplicates giving the same results. Shown here are representative blots.

## BN-PAGE

BN-PAGE experiments of total enriched chloroplast membrane fractions were carried out as described by (Nickel et al., 2016), with minor modifications. Samples equal to 15 μg chl were solubilized with 5% β-dodecylmaltoside for 15 min and separated on a 5%–15% acrylamide gradient overnight. For subsequent western blotting, lanes were incubated in Towbin buffer [25 mM Tris pH 8.3, 192 mM glycine, 0.1% (w/v) SDS, 20% (v/v) MeOH] with additional 0.9% (w/v) SDS for 1 h prior to blotting. For 2D experiments, the respective BN gel lane was incubated for 30 min in BN-denaturation buffer (1% (w/v) SDS, 50 mM DTT, 25 mM Tris, 192 mM glycine), washed, and afterward assembled on top of an SDS–PAGE. Total enriched chloroplast membrane fractions equal to 15 μg chl were loaded as a control and separated on the same SDS–PAGE.

## Photosynthetic parameters and chlorophyll quantification

Plants were dark-adapted for 20 min. Subsequently, chlorophyll *a* fluorescence was measured with a Walz IMAGING-PAM M-Series MAXI version (Walz, Effeltrich, Germany). False-color images were exported using the ImagingWinGigE software. Total chlorophyll was extracted from 5 to 10 mg of $N_2$-frozen powderized plant material in prechilled reaction tubes. After addition of 1 mL 80% (v/v) acetone, samples were incubated for at least 30 min on ice in the dark interrupted by occasional vortexing. Samples were centrifuged at 10,000*g* for 5 min at 4°C to pellet debris. Chlorophyll determination was performed trough photometry on the clear supernatant (Porra et al., 1989). Obtained values were normalized to fresh weight, and then to the WT. A representative result of three independent experiments is shown.

## Generation of stable Aequorin reporter mutants and $Ca^{2+}$ assays

Aequorin lines were generated by using the floral dip method with *A. tumefaciens* strains harboring the plasmid pBINU-CHYA(K) (Mehlmer et al., 2012). Homozygous $T_3$ individuals were introgressed into mutant lines and homozygosity of the reporter lines was confirmed in the $F_3$ generation. Aequorin assays were performed according to (Tanaka et al., 2013), with minor changes to the CTZ buffer. In brief, 5-d-old seedlings were transferred from 1/2 MS plates to white 96-well plates filled with 50 μL CTZ buffer (1.4 mM $CaCl_2$, 20 mM KCl, 5 mM MES pH5.7) containing 10 μM coelenterazine (NanoLight Technologies, USA, CAS#55779-48-1). Seedlings were kept in the dark overnight at 22°C. Luminescence was recorded in a TECAN SPARK plate reader (Tecan, Männedorf, Switzerland) with 500 ms integration time (400 ms in supplementary experiments). Total, reconstituted AEQUORIN amounts were calculated by discharging with 10% (v/v) ethanol and 1 M $CaCl_2$. Calibrations were performed according to (Knight et al., 1996). Graphs were plotted with GraphPad Prism. A representative result of at least three experiments is shown. Statistical significance was tested using analysis of variance followed by Tukey's multiple comparisons test.

## Elemental analysis

Leaf elements are analyzed by Total Reflection X-ray Fluorescence (TXRF) spectroscopy. All procedures were previously described in detail (Höhner et al., 2016). In brief, 21-d-old plants were harvested, pooled in groups of three, and dried completely in an oven at 80°C. To avoid elemental contamination, tissue was ground into fine powder using a zirconia mortar and pestle (Stanford Advanced Materials, Lake Forest, USA). A 5–10 mg dry weight tissue was digested by boiling in 1 mL 70% (v/v) $HNO_3$ (analytical grade). About 100 μL of the digested tissue was mixed with internal quantitative Ga and Sc standards to final concentrations of 1 ppm Ga and 50 ppm Sc. A mixture of 10 μL was spotted

onto quartz disc carriers and dried before measuring on a S4 T-STAR TXRF spectrometer (Bruker, Berlin, Germany).

### Accession numbers

*PEC1* (At5g02940), *PEC2* (At5g43745), *DMI1* (At5g49960), *TIC40* (At5g16620), *NTRC* (AT2G41680), *pec1-1* (SAIL_300_A10, CS72537), *pec1-2* (SALK_045095, CS72538), *pec2-1* (SALK_102200, CS72539), *pec2-2* (SAIL_839_E05, CS72540), *pec1-1pec2-1* (CS72541), *pec1-2pec2-2* (CS72542), *cas-1* (SALK_070416), Col-0 WT NTRC-YFP-AEQ (CS72534), *pec1-1pec2-1* NTRC-YFP-AEQ (CS72535), *pec1-2pec2-2* NTRC-YFP-AEQ (CS72536).

## Supplemental data

The following materials are available in the online version of this article.

**Supplementary Figure S1**. Phylogeny of PEC, CASTOR, and POLLUX homologs.

**Supplemental Figure S2**. PEC domains and construct information.

**Supplemental Figure S3**. Localization studies of PEC proteins in *N. benthamiana* and *Arabidopsis thaliana*.

**Supplemental Figure S4**. α-PEC1 antibody design and application in localization studies.

**Supplemental Figure S5**. Extended PEC expression information.

**Supplemental Figure S6**. *PEC* locus information and *pec* single mutant characterization.

**Supplemental Figure S7**. Background AEQUORIN and additional cold shock measurements, single mutant readings, and complementation by backcross into the WT.

**Supplemental Figure S8**. Lack of stromal $Ca^{2+}$ transients in *pec1pec2* mutants does not correspond with additional growth defects under abiotic stress conditions.

**Supplemental Table S1**. Oligonucleotide combinations used in genotyping PCRs.

**Supplemental Table S2**. List of oligonucleotides used in this study.

**Supplemental Table S3**. Constructs used in this study and their origin.

**Supplemental Dataset S1**. Main Figure 1 alignment

**Supplemental Dataset S2**. Supplemental Figure S1 alignment.

## Acknowledgments

We thank Prof. Ute Vothknecht (University of Bonn) for kindly providing NTRC-YA vector DNA and the respective Arabidopsis $Ca^{2+}$ reporter line. We thank Dr. Myriam Charpentier (John Innes Centre) for early advice on the yeast $K^+$ assays and Dr Sychrová Hana (Czech Academy of Sciences at Prague) for sharing the MAB2d mutant strain. Many thanks to Drs Michael Varnum (Washington State University) and Miguel Piñeros (Cornell University) for tremendous support in trying to establish electrophysiology assays on PECs in Xenopus ooyctes. We are very thankful for many helpful aequorin-related discussions with Drs Tanaka and Jewell (both WSU) and their insights on plate-reader-based luminescence assays. Lots of thanks to A.H. Howell for confocal microscopy assistance, to Dr DeTar for help in ionomics sample preparation and evaluation, to A.I. Pratt (all WSU) for early discussions on $Ca^{2+}$ assays, and to Dr Jordan Zager (Dewey Scientific) for discussion on various parts of the project. C.M. and C.L. Lewis (Alumni WSU Honors College), and K. Bünger (LMU Munich) supported various aspects of the projects. A.M. Garbers (WSU) assisted early in the project. C.V. is grateful for travel support through the WSU Elling and Higinbotham scholarship program and support for microscopy work through the WSU Franceschi training grant.

## Funding

H.-H.K. received funding from an National Science Foundation (NSF) Career Award (IOS-1553506) and a third call ERA-CAPS grant from NSF (IOS-1847382). Elemental analysis was realized through an NSF MRI-1828266 award to H.-H.K. B.B. received funding from the Deutsche Forschungsgemeinschaft (DFG) (SFB-TR 175, project B06). Work in the lab of J.d.V. is supported through funding from the European Research Council (ERC) under the European Union's Horizon 2020 research and innovation program (grant no. 852725; ERC Starting Grant 'TerreStriAL'). A.D.A. and J.d.V. are part of the framework of MAdLand (http://madland.science, DFG priority program 2237), J.d.V. is grateful for funding by the DFG (VR132/4-1).

*Conflict of interest statement*. None declared.

## References

**Amborella Genome P** (2013) The Amborella genome and the evolution of flowering plants. Science **342:** 1241089

**Aranda-Sicilia MN, Cagnac O, Chanroj S, Sze H, Rodriguez-Rosales MP, Venema K** (2012) Arabidopsis KEA2, a homolog of bacterial KefC, encodes a K( + )/H( + ) antiporter with a chloroplast transit peptide. Biochim Biophys Acta **1818:** 2362–2371

**Aranda Sicilia MN, Sanchez Romero ME, Rodriguez Rosales MP, Venema K** (2021) Plastidial transporters KEA1 and KEA2 at the inner envelope membrane adjust stromal pH in the dark. New Phytol **229:** 2080–2090

**Arino J, Velazquez D, Casamayor A** (2019) Ser/Thr protein phosphatases in fungi: structure, regulation and function. Microb Cell **6:** 217–256

**Banks JA, Nishiyama T, Hasebe M, Bowman JL, Gribskov M, dePamphilis C, Albert VA, Aono N, Aoyama T, Ambrose BA, et al.** (2011) The Selaginella genome identifies genetic changes associated with the evolution of vascular plants. Science **332:** 960–963

**Benz JP, Stengel A, Lintala M, Lee YH, Weber A, Philippar K, Gugel IL, Kaieda S, Ikegami T, Mulo P, et al.** (2009) Arabidopsis Tic62 and ferredoxin-NADP(H) oxidoreductase form light-regulated complexes that are integrated into the chloroplast redox poise. Plant Cell **21:** 3965–3983

**Bernardi P** (1999) Mitochondrial transport of cations: channels, exchangers, and permeability transition. Physiol Rev **79:** 1127–1155

**Blanc G, Agarkova I, Grimwood J, Kuo A, Brueggeman A, Dunigan DD, Gurnon J, Ladunga I, Lindquist E, Lucas S, et al.** (2012) The genome of the polar eukaryotic microalga Coccomyxa

subellipsoidea reveals traits of cold adaptation. Genome Biol **13:** R39

**Bolter B, Mitterreiter MJ, Schwenkert S, Finkemeier I, Kunz HH** (2020) The topology of plastid inner envelope potassium cation efflux antiporter KEA1 provides new insights into its regulatory features. Photosynth Res **145:** 43–54

**Bouchnak I, Brugiere S, Moyet L, Le Gall S, Salvi D, Kuntz M, Tardif M, Rolland N** (2019) Unraveling hidden components of the chloroplast envelope proteome: opportunities and limits of better MS sensitivity. Mol Cell Proteomics **18:** 1285–1306

**Bowman JL, Kohchi T, Yamato KT, Jenkins J, Shu S, Ishizaki K, Yamaoka S, Nishihama R, Nakamura Y, Berger F, et al.** (2017) Insights into land plant evolution garnered from the marchantia polymorpha genome. Cell **171:** 287–304 e215

**Brautigam A, Hoffmann-Benning S, Weber AP** (2008) Comparative proteomics of chloroplast envelopes from C3 and C4 plants reveals specific adaptations of the plastid envelope to C4 photosynthesis and candidate proteins required for maintaining C4 metabolite fluxes. Plant Physiol **148:** 568–579

**Charpentier M, Bredemeier R, Wanner G, Takeda N, Schleiff E, Parniske M** (2008) Lotus japonicus CASTOR and POLLUX are ion channels essential for perinuclear calcium spiking in legume root endosymbiosis. Plant Cell **20:** 3467–3479

**Charpentier M, Sun J, Vaz Martins T, Radhakrishnan GV, Findlay K, Soumpourou E, Thouin J, Very AA, Sanders D, Morris RJ, Oldroyd GE** (2016) Nuclear-localized cyclic nucleotide-gated channels mediate symbiotic calcium oscillations. Science **352:** 1102–1105

**Cheng S, Xian W, Fu Y, Marin B, Keller J, Wu T, Sun W, Li X, Xu Y, Zhang Y, et al.** (2019) Genomes of subaerial zygnematophyceae provide insights into land plant evolution. Cell **179:** 1057–1067 e1014

**Clausen C, Ilkavets I, Thomson R, Philippar K, Vojta A, Mohlmann T, Neuhaus E, Fulgosi H, Soll J** (2004) Intracellular localization of VDAC proteins in plants. Planta **220:** 30–37

**Clough SJ, Bent AF** (1998) Floral dip: a simplified method for Agrobacterium-mediated transformation of Arabidopsis thaliana. Plant J **16:** 735–743

**de Clerck O, Kao SM, Bogaert KA, Blomme J, Foflonker F, Kwantes M, Vancaester E, Vanderstraeten L, Aydogdu E, Boesger J, et al.** (2018) Insights into the evolution of multicellularity from the sea lettuce genome. Curr Biol **28:** 2921–2933 e2925

**deTar RA, Barahimipour R, Manavski N, Schwenkert S, Höhner R, Bölter B, Inaba T, Meurer J, Zoschke R, Kunz H-H** (2021) Loss of inner-envelope K + /H + exchangers impairs plastid rRNA maturation and gene expression. Plant Cell **33**: 2479–2505

**de Vries J, Curtis BA, Gould SB, Archibald JM** (2018) Embryophyte stress signaling evolved in the algal progenitors of land plants. Proc Natl Acad Sci U S A **115:** E3471–E3480

**de Vries J, de Vries S, Curtis BA, Zhou H, Penny S, Feussner K, Pinto DM, Steinert M, Cohen AM, von Schwartzenberg K, et al.** (2020) Heat stress response in the closest algal relatives of land plants reveals conserved stress signaling circuits. Plant J **103:** 1025–1048

**Dohm JC, Minoche AE, Holtgrawe D, Capella-Gutierrez S, Zakrzewski F, Tafer H, Rupp O, Sorensen TR, Stracke R, Reinhardt R, et al.** (2014) The genome of the recently domesticated crop plant sugar beet (Beta vulgaris). Nature **505:** 546–549

**Eisenhut M, Hoecker N, Schmidt SB, Basgaran RM, Flachbart S, Jahns P, Eser T, Geimer S, Husted S, Weber APM, Leister D, Schneider A** (2018) The plastid envelope CHLOROPLAST MANGANESE TRANSPORTER1 is essential for manganese homeostasis in Arabidopsis. Mol Plant **11:** 955–969

**Flores-Perez U, Jarvis P** (2017) Isolation and suborganellar fractionation of Arabidopsis Chloroplasts. Methods Mol Biol **1511:** 45–60

**Frank J, Happeck R, Meier B, Hoang MTT, Stribny J, Hause G, Ding H, Morsomme P, Baginsky S, Peiter E** (2019) Chloroplast-localized BICAT proteins shape stromal calcium signals and are required for efficient photosynthesis. New Phytol **221:** 866–880

**Froehlich J** (2011) Studying Arabidopsis envelope protein localization and topology using thermolysin and trypsin proteases. Methods Mol Biol **774:** 351–367

**Furst-Jansen JMR, de Vries S, de Vries J** (2020) Evo-physio: on stress responses and the earliest land plants. J Exp Bot **71:** 3254–3269

**Gietz RD, Woods RA** (2001) Genetic transformation of yeast. Biotechniques **30:** 816–820, 822–816, 828 passim

**Gutierrez-Carbonell E, Takahashi D, Lattanzio G, Rodriguez-Celma J, Kehr J, Soll J, Philippar K, Uemura M, Abadia J, Lopez-Millan AF** (2014) The distinct functional roles of the inner and outer chloroplast envelope of Pea (*Pisum sativum*) as revealed by proteomic approaches. J Proteome Res **13:** 2941–2953

**Hoang DT, Chernomor O, von Haeseler A, Minh BQ, Vinh LS** (2018) UFBoot2: improving the ultrafast bootstrap approximation. Mol Biol Evol **35:** 518–522

**Höhner R, Day PM, Zimmermann SE, Lopez LS, Krämer M, Giavalisco P, Correa Galvis V, Armbruster U, Schöttler MA, Jahns P, et al.** (2021) Stromal NADH supplied by PHOSPHOGLYCERATE DEHYDROGENASE3 is crucial for photosynthetic performance. Plant Physiol **186**: 142–167

**Höhner R, Galvis VC, Strand DD, Völkner C, Kramer M, Messer M, Dinc F, Sjuts I, Bolter B, Kramer DM, et al.** (2019) Photosynthesis in Arabidopsis Is Unaffected by the Function of the Vacuolar K($^+$) Channel TPK3. Plant Physiol **180:** 1322–1335

**Höhner R, Tabatabaei S, Kunz H-H, Fittschen U** (2016) A rapid total reflection X-ray fluorescence protocol for micro analyses of ion profiles in Arabidopsis thaliana. Spectrochimica Acta Part B: Atomic Spectroscopy **125:** 159–167

**Hori K, Maruyama F, Fujisawa T, Togashi T, Yamamoto N, Seo M, Sato S, Yamada T, Mori H, Tajima N, et al.** (2014) Klebsormidium flaccidum genome reveals primary factors for plant terrestrial adaptation. Nat Commun **5:** 3978

**Hu TT, Pattyn P, Bakker EG, Cao J, Cheng JF, Clark RM, Fahlgren N, Fawcett JA, Grimwood J, Gundlach H, et al.** (2011) The *Arabidopsis lyrata* genome sequence and the basis of rapid genome size change. Nat Genet **43:** 476–481

**Imaizumi-Anraku H, Takeda N, Charpentier M, Perry J, Miwa H, Umehara Y, Kouchi H, Murakami Y, Mulder L, Vickers K, et al.** (2005) Plastid proteins crucial for symbiotic fungal and bacterial entry into plant roots. Nature **433:** 527–531

International Brachypodium I (2010) Genome sequencing and analysis of the model grass Brachypodium distachyon. Nature **463:** 763–768

**Jiao C, Sorensen I, Sun X, Sun H, Behar H, Alseekh S, Philippe G, Palacio Lopez K, Sun L, Reed R, et al.** (2020) The penium margaritaceum genome: hallmarks of the origins of land plants. Cell **181:** 1097–1111 e1012

**Ju C, Van de Poel B, Cooper ED, Thierer JH, Gibbons TR, Delwiche CF, Chang C** (2015) Conservation of ethylene as a plant hormone over 450 million years of evolution. Nat Plants **1:** 14004

**Kalyaanamoorthy S, Minh BQ, Wong TKF, von Haeseler A, Jermiin LS** (2017) ModelFinder: fast model selection for accurate phylogenetic estimates. Nat Methods **14:** 587–589

**Katoh K, Standley DM** (2013) MAFFT multiple sequence alignment software version 7: improvements in performance and usability. Mol Biol Evol **30:** 772–780

**Kilian J, Whitehead D, Horak J, Wanke D, Weinl S, Batistic O, D'Angelo C, Bornberg-Bauer E, Kudla J, Harter K** (2007) The AtGenExpress global stress expression data set: protocols, evaluation and model data analysis of UV-B light, drought and cold stress responses. Plant J **50:** 347–363

**Kim S, Zeng W, Bernard S, Liao J, Venkateshwaran M, Ane JM, Jiang Y** (2019) Ca($^{2+}$)-regulated Ca($^{2+}$) channels with an RCK gating ring control plant symbiotic associations. Nat Commun **10:** 3703

**Knight H, Trewavas AJ, Knight MR** (1996) Cold calcium signaling in Arabidopsis involves two cellular pools and a change in calcium signature after acclimation. Plant Cell **8:** 489–503

**Kreplak J, Madoui MA, Capal P, Novak P, Labadie K, Aubert G, Bayer PE, Gali KK, Syme RA, Main D, et al.** (2019) A reference genome for pea provides insight into legume genome evolution. Nat Genet **51:** 1411–1422

**Kunz HH, Gierth M, Herdean A, Satoh-Cruz M, Kramer DM, Spetea C, Schroeder JI** (2014) Plastidial transporters KEA1, -2, and -3 are essential for chloroplast osmoregulation, integrity, and pH regulation in Arabidopsis. Proc Natl Acad Sci U S A **111:** 7480–7485

**Lamesch P, Berardini TZ, Li D, Swarbreck D, Wilks C, Sasidharan R, Muller R, Dreher K, Alexander DL, Garcia-Hernandez M, et al.** (2012) The Arabidopsis Information Resource (TAIR): improved gene annotation and new tools. Nucleic Acids Res **40:** D1202–1210

**Lang D, Ullrich KK, Murat F, Fuchs J, Jenkins J, Haas FB, Piednoel M, Gundlach H, Van Bel M, Meyberg R, et al.** (2018) The Physcomitrella patens chromosome-scale assembly reveals moss genome structure and evolution. Plant J **93:** 515–533

**Le SQ, Gascuel O** (2008) An improved general amino acid replacement matrix. Mol Biol Evol **25:** 1307–1320

**Leitao N, Dangeville P, Carter R, Charpentier M** (2019) Nuclear calcium signatures are associated with root development. Nat Commun **10:** 4865

**Lenzoni G, Knight MR** (2019) Increases in absolute temperature stimulate free calcium concentration elevations in the chloroplast. Plant Cell Physiol **60:** 538–548

**Li FW, Nishiyama T, Waller M, Frangedakis E, Keller J, Li Z, Fernandez-Pozo N, Barker MS, Bennett T, Blazquez MA, et al.** (2020) Anthoceros genomes illuminate the origin of land plants and the unique biology of hornworts. Nat Plants **6:** 259–272

**Li H, Jiang F, Wu P, Wang K, Cao Y** (2020) A high-quality genome sequence of model legume lotus japonicus (MG-20) provides insights into the evolution of root nodule symbiosis. Genes (Basel) **11**: 483

**Maresova L, Sychrova H** (2005) Physiological characterization of Saccharomyces cerevisiae kha1 deletion mutants. Mol Microbiol **55:** 588–600

**Marti Ruiz MC, Jung HJ, Webb AAR** (2020) Circadian gating of dark-induced increases in chloroplast- and cytosolic-free calcium in Arabidopsis. New Phytol **225:** 1993–2005

**Mehlmer N, Parvin N, Hurst CH, Knight MR, Teige M, Vothknecht UC** (2012) A toolset of aequorin expression vectors for in planta studies of subcellular calcium concentrations in Arabidopsis thaliana. J Exp Bot **63:** 1751–1761

**Merchant SS, Prochnik SE, Vallon O, Harris EH, Karpowicz SJ, Witman GB, Terry A, Salamov A, Fritz-Laylin LK, Marechal-Drouard L, et al.**, (2007) The chlamydomonas genome reveals the evolution of key animal and plant functions. Science **318:** 245–250

**Mi F, Peters JS, Berkowitz GA** (1994) Characterization of a chloroplast inner envelope $K^+$ channel. Plant Physiol **105:** 955–964

**Minh BQ, Schmidt HA, Chernomor O, Schrempf D, Woodhams MD, von Haeseler A, Lanfear R** (2020) IQ-TREE 2: new models and efficient methods for phylogenetic inference in the genomic era. Mol Biol Evol **37:** 1530–1534

**Nickel C, Brylok T, Schwenkert S** (2016) In vivo radiolabeling of arabidopsis chloroplast proteins and separation of thylakoid membrane complexes by blue native PAGE. Methods Mol Biol **1450:** 233–245

**Nishiyama T, Sakayama H, de Vries J, Buschmann H, Saint-Marcoux D, Ullrich KK, Haas FB, Vanderstraeten L, Becker D, Lang D, et al.**, (2018) The Chara genome: secondary complexity and implications for plant terrestrialization. Cell **174:** 448–464 e424[PMC][30007417]

**Nomura H, Komori T, Uemura S, Kanda Y, Shimotani K, Nakai K, Furuichi T, Takebayashi K, Sugimoto T, Sano S, et al.** (2012) Chloroplast-mediated activation of plant immune signalling in Arabidopsis. Nat Commun **3:** 926

**Ouyang S, Zhu W, Hamilton J, Lin H, Campbell M, Childs K, Thibaud-Nissen F, Malek RL, Lee Y, Zheng L, et al.** (2007) The TIGR rice genome annotation resource: improvements and new features. Nucleic Acids Res **35:** D883–D887

**Porra RJ, Thompson WA, Kriedemann PE** (1989) Determination of accurate extinction coefficients and simultaneous equations for assaying chlorophylls a and b extracted with four different solvents: verification of the concentration of chlorophyll standards by atomic absorption spectroscopy. Biochimica et Biophysica Acta (BBA)-Bioenergetics **975:** 384–394

**Pottosin, II, Muniz J, Shabala S** (2005) Fast-activating channel controls cation fluxes across the native chloroplast envelope. J Membr Biol **204:** 145–156

**Pottosin I, Dobrovinskaya O** (2015) Ion channels in native chloroplast membranes: challenges and potential for direct patch-clamp studies. Front Physiol **6:** 396

**Pratt AI, Knoblauch J, Kunz HH** (2020) An updated pGREEN-based vector suite for cost-effective cloning in plant molecular biology. MicroPubl Biol **2020**

**Resentini F, Ruberti C, Grenzi M, Bonza MC, Costa A** (2021) The signatures of organellar calcium. Plant Physiol **187**: 1985–2004

**Roy A, Kucukural A, Zhang Y** (2010) I-TASSER: a unified platform for automated protein structure and function prediction. Nat Protoc **5:** 725–738

**Schwacke R, Schneider A, van der Graaff E, Fischer K, Catoni E, Desimone M, Frommer WB, Flugge UI, Kunze R** (2003) ARAMEMNON, a novel database for Arabidopsis integral membrane proteins. Plant Physiol **131:** 16–26

**Shikanai T, Muller-Moule P, Munekage Y, Niyogi KK, Pilon M** (2003) PAA1, a P-type ATPase of Arabidopsis, functions in copper transport in chloroplasts. Plant Cell **15:** 1333–1346

**Sohrt K, Soll J** (2000) Toc64, a new component of the protein translocon of chloroplasts. J Cell Biol **148:** 1213–1221

**Stahl T, Glockmann C, Soll J, Heins L** (1999) Tic40, a new "old" subunit of the chloroplast protein import translocon. J Biol Chem **274:** 37467–37472

**Sun Q, Zybailov B, Majeran W, Friso G, Olinares PD, van Wijk KJ** (2009) PPDB, the plant proteomics database at Cornell. Nucleic Acids Res **37:** D969–D974

**Tanaka K, Choi J, Stacey G** (2013) Aequorin luminescence-based functional calcium assay for heterotrimeric G-proteins in Arabidopsis. Methods Mol Biol **1043:** 45–54

**Teardo E, Carraretto L, Moscatiello R, Cortese E, Vicario M, Festa M, Maso L, De Bortoli S, Cali T, Vothknecht UC, et al.**, (2019) A chloroplast-localized mitochondrial calcium uniporter transduces osmotic stress in Arabidopsis. Nat Plants **5:** 581–588

**Trentmann O, Muhlhaus T, Zimmer D, Sommer F, Schroda M, Haferkamp I, Keller I, Pommerrenig B, Neuhaus HE** (2020) Identification of chloroplast envelope proteins with critical importance for cold acclimation. Plant Physiol **182:** 1239–1255

**Tsujii M, Kera K, Hamamoto S, Kuromori T, Shikanai T, Uozumi N** (2019) Evidence for potassium transport activity of Arabidopsis KEA1-KEA6. Sci Rep **9:** 10040

**Venkateshwaran M, Cosme A, Han L, Banba M, Satyshur KA, Schleiff E, Parniske M, Imaizumi-Anraku H, Ane JM** (2012) The recent evolution of a symbiotic ion channel in the legume family altered ion conductance and improved functionality in calcium signaling. Plant Cell **24:** 2528–2545

**Voinnet O, Rivas S, Mestre P, Baulcombe D** (2003) An enhanced transient expression system in plants based on suppression of gene silencing by the p19 protein of tomato bushy stunt virus. Plant J **33:** 949–956

**Waadt R, Schlucking K, Schroeder JI, Kudla J** (2014) Protein fragment bimolecular fluorescence complementation analyses for the in vivo study of protein-protein interactions and cellular protein complex localizations. Methods Mol Biol **1062:** 629–658

**Wan T, Liu ZM, Li LF, Leitch AR, Leitch IJ, Lohaus R, Liu ZJ, Xin HP, Gong YB, Liu Y, et al.** (2018) A genome for gnetophytes and early evolution of seed plants. Nat Plants **4:** 82–89

**Wang S, Li L, Li H, Sahu SK, Wang H, Xu Y, Xian W, Song B, Liang H, Cheng S, et al.** (2020) Genomes of early-diverging streptophyte algae shed light on plant terrestrialization. Nat Plants **6:** 95–106

**Wang X, Berkowitz GA, Peters JS** (1993) $K^+$-conducting ion channel of the chloroplast inner envelope: functional reconstitution into liposomes. Proc Natl Acad Sci U S A **90:** 4981–4985

**Weinl S, Held K, Schlucking K, Steinhorst L, Kuhlgert S, Hippler M, Kudla J** (2008) A plastid protein crucial for $Ca^{2+}$-regulated stomatal responses. New Phytol **179:** 675–686

**Whelan S, Goldman N** (2001) A general empirical model of protein evolution derived from multiple protein families using a maximum-likelihood approach. Mol Biol Evol **18:** 691–699

**Worden AZ, Lee JH, Mock T, Rouze P, Simmons MP, Aerts AL, Allen AE, Cuvelier ML, Derelle E, Everett MV, et al.** (2009) Green evolution and dynamic adaptations revealed by genomes of the marine picoeukaryotes Micromonas. Science **324:** 268–272

**Wu W, Peters J, Berkowitz GA** (1991) Surface charge-mediated effects of mg on K flux across the chloroplast envelope are associated with regulation of stromal pH and photosynthesis. Plant Physiol **97:** 580–587

**Zhang B, Zhang C, Liu C, Jing Y, Wang Y, Jin L, Yang L, Fu A, Shi J, Zhao F, et al.** (2018) Inner Envelope CHLOROPLAST MANGANESE TRANSPORTER 1 supports manganese homeostasis and phototrophic growth in Arabidopsis. Mol Plant **11:** 943–954

**Zhang H, Zhang F, Yu Y, Feng L, Jia J, Liu B, Li B, Guo H, Zhai J** (2020) A comprehensive online database for exploring approximately 20,000 public Arabidopsis RNA-Seq libraries. Mol Plant **13:** 1231–1233